Supplement of Atmos. Chem. Phys., 20, 14321–14332, 2020
https://doi.org/10.5194/acp-20-14321-2020-supplement

Atmospheric Chemistry and Physics
Open Access
EGU

Supplement of

Tracing the evolution of morphology and mixing state of soot particles along with the movement of an Asian dust storm

Liang Xu et al.

Correspondence to: Weijun Li (liweijun@zju.edu.cn)

1. Information about samples and the Asian dust storm event

Table S1. Detailed information about sampling dates, times, meteorological conditions, and PM concentrations for samples.

	Sample ID	Date	Sampling Time (UTC)	Sampling duration Second	Temp °C	RH %	Pressure hPa	Wind Direction °	Wind speed m/s	PM_{10}/ $PM_{2.5}$ μg/m^3	Particle No.
Jinan (T1)	dust-1	3-18	02:27	60	-	-	-	179	3.9	526/98	412
	dust-2	3-18	02:28	50	-	-	-	357	2.4		
	dust-3	3-18	02:40	100	-	-	-	89	1.7		
Qingdao (T2)	dust-1	3-17	23:54	90	12.5	49.5	1013.3	278	0.7	490/140	486
	dust-2	3-18	12:00	120	8.4	79.3	1013.6	162	1.3	153/55	
Amakusa (T3)	dust-1	3-18	15:16	120	16.2	85.1	1013	121	1.1	63/52	887
	dust-2	3-18	22:36	60	13.7	92.2	1012.6	358	0.6	54/47	

The dust total concentration in Figure S1 clearly shows that at 00:00 on 2014/03/18 (UTC), the dust storm has already passed T1 and T2, heading eastwards (wind arrows) to reach T3. The mean sea level pressure and wind vectors in Figure S2 could also confirm the movement of this high pressure system (yellow) on 03/17, 03/18, and 03/19.

The air behind a cold front is colder and drier than the air in front. When the cold front passes through, the RH and temperature can drop, and the pressure can increase. Based on this and Figure S3-S5, we can define the time of the cold front passage. The cold front arrived T1 around 06:00 on 03/17, T2 at 09:00 on 03/17, and T3 at 02:00 on 03/18 (UTC). This is consistent with the arrival time derived from the PM concentration in Figure 1b.

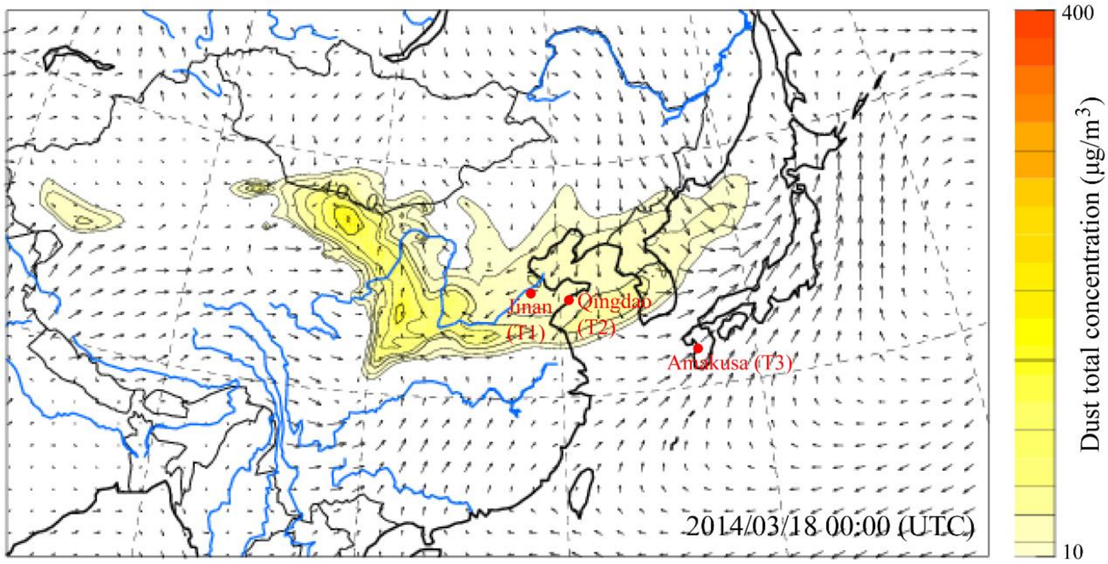

Figure S1. Distributions of dust in East Asian region at 2014/03/18. Data is provided by the National Institute for Environment Studies and Kyushu University (http://www-cfors.nies.go.jp/~cfors/).

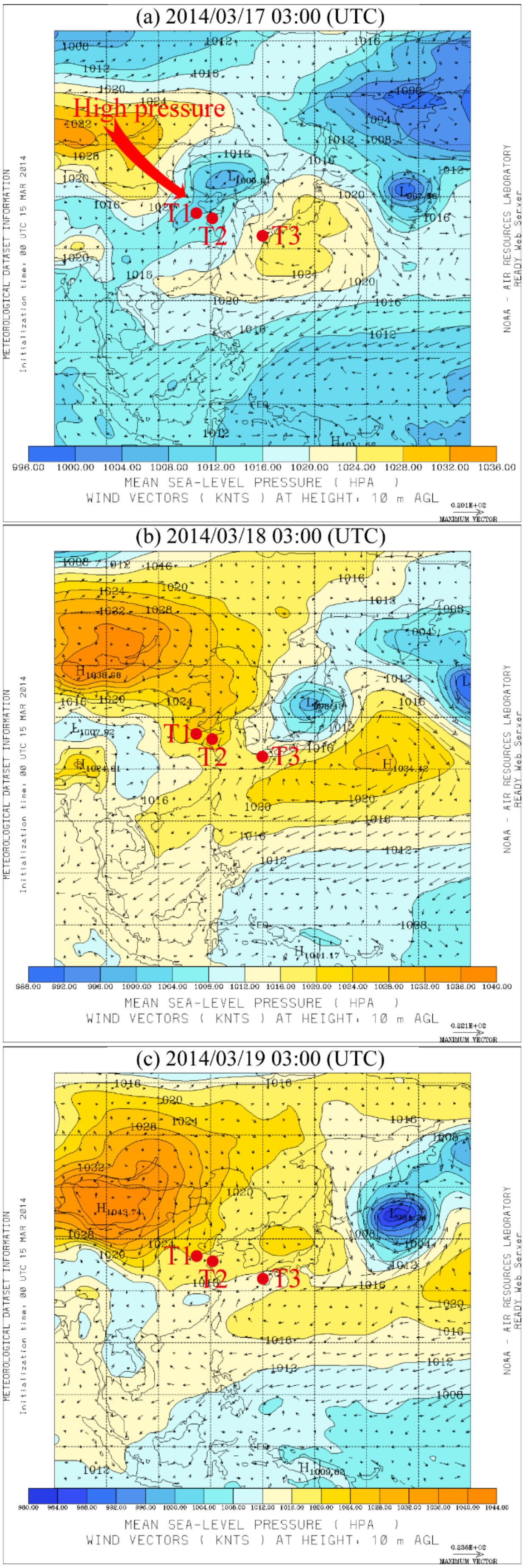
(a) 2014/03/17 03:00 (UTC)
High pressure
T1
T2
T3
METEOROLOGICAL DATASET INFORMATION
Initialization time: 00 UTC 15 MAR 2014
NOAA - AIR RESOURCES LABORATORY
READY Web Server
MEAN SEA-LEVEL PRESSURE (HPA)
WIND VECTORS (KNTS) AT HEIGHT: 10 m AGL
MAXIMUM VECTOR
(b) 2014/03/18 03:00 (UTC)
T1
T2
T3
METEOROLOGICAL DATASET INFORMATION
Initialization time: 00 UTC 15 MAR 2014
NOAA - AIR RESOURCES LABORATORY
READY Web Server
MEAN SEA-LEVEL PRESSURE (HPA)
WIND VECTORS (KNTS) AT HEIGHT: 10 m AGL
MAXIMUM VECTOR
(c) 2014/03/19 03:00 (UTC)
T1
T2
T3
METEOROLOGICAL DATASET INFORMATION
Initialization time: 00 UTC 15 MAR 2014
NOAA - AIR RESOURCES LABORATORY
READY Web Server
MEAN SEA-LEVEL PRESSURE (HPA)
WIND VECTORS (KNTS) AT HEIGHT: 10 m AGL
MAXIMUM VECTOR

Figure S2. The mean sea level pressure (hPa) and wind vectors (knots) at 03/17, 03/18, and 03/19 at the three sampling sites. Data source: NOAA Air Resources Laboratory's (ARL) Real-time Environmental Applications and Display sYstem (READY) (Rolph et al., 2017).

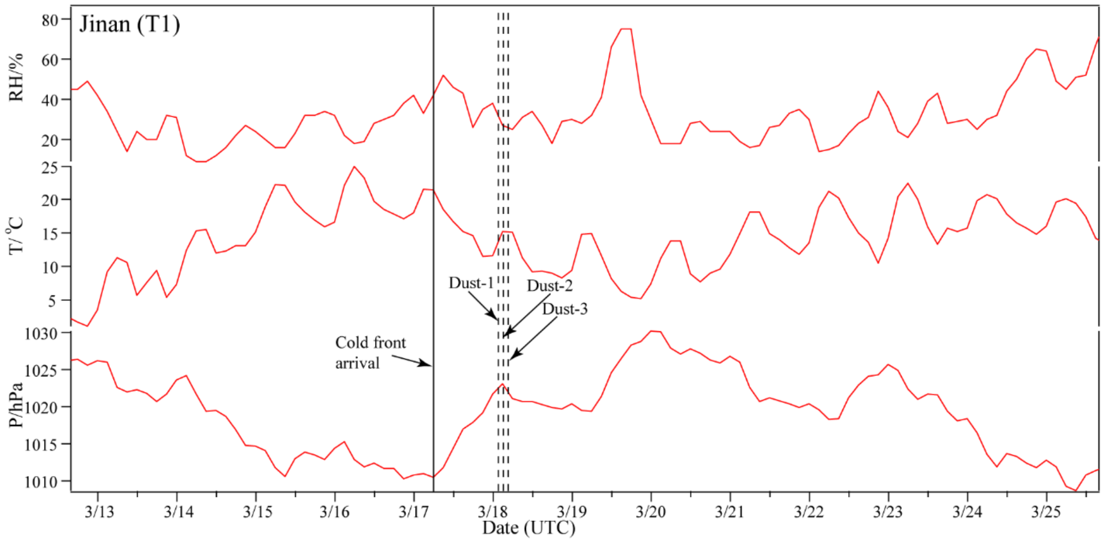

Figure S3. Time series of surface weather conditions: relative humidity (RH), temperature (T), and pressure (P) at Jinan (T1). The start time of the cold front passage is marked by the solid line. Collection time of dust samples is marked by the dash lines. Data source: the National Oceanic and Atmospheric Administration (NOAA).

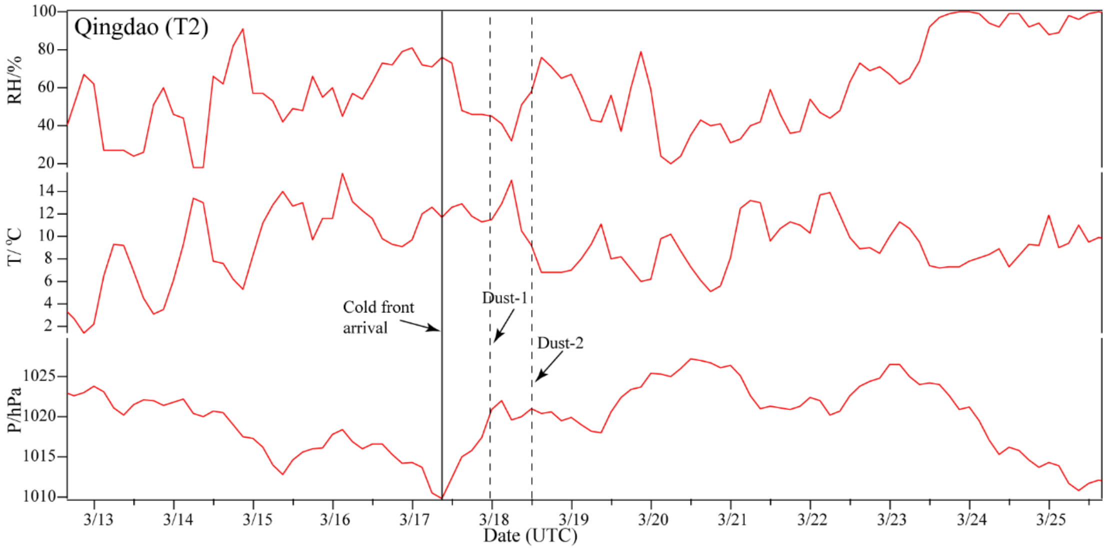

Figure S4. Time series of surface weather conditions: relative humidity (RH), temperature (T), and pressure (P) at Qingdao (T2). Data source: the National Oceanic and Atmospheric Administration (NOAA).

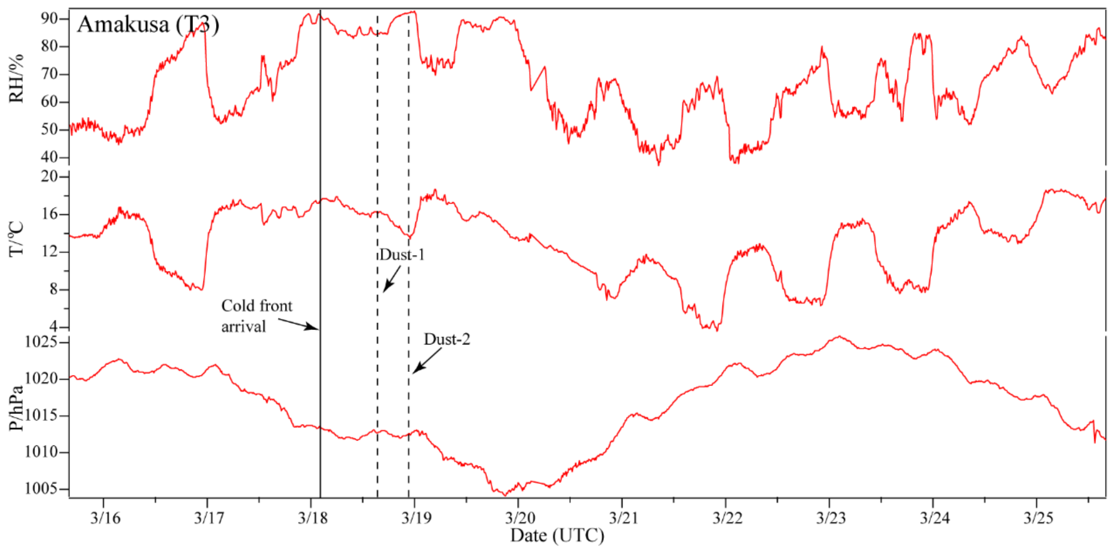

Figure S5. Time series of surface weather conditions: relative humidity (RH), temperature (T), and pressure (P) at Amakusa (T3).

2. The correlation between EVD and ECD obtained by AFM

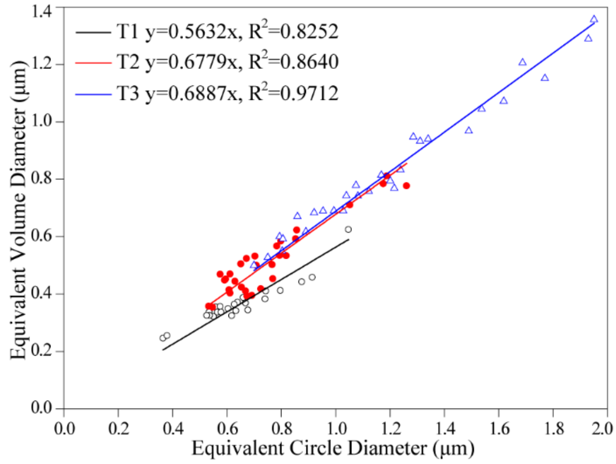

Figure S6. The correlation of equivalent circle diameter (ECD) and equivalent volume diameter (EVD) at three sampling sites obtained by AFM.

$$A=\pi r^2=\pi\times\left(\frac{d}{2}\right)^2=\frac{\pi d^2}{4} \longrightarrow d=\sqrt{\frac{4A}{\pi}} \tag{1}$$

$$V=\frac{4}{3}\pi r^3=\frac{4}{3}\times\frac{\pi D^3}{8}=\frac{\pi D^3}{6} \longrightarrow D=\sqrt[3]{\frac{6V}{\pi}} \tag{2}$$

where d is the equivalent circle diameter (ECD) and D the equivalent volume diameter (EVD) (Chi et al., 2015).

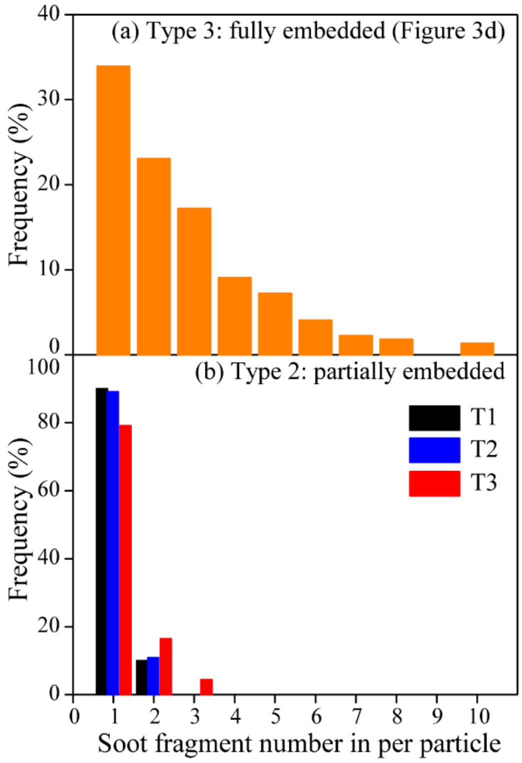

Figure S7. Frequency of soot fragment number in single soot-bearing particles.

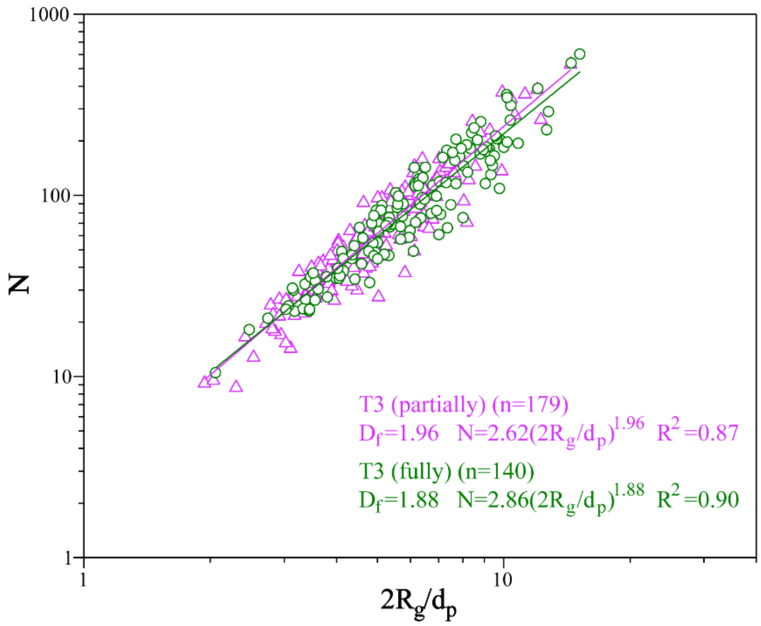

Figure S8. Fractal dimension of partially and fully embedded soot particles at T3 site. It is different to provide fractal dimension of different types of soot at T1 and T2 because of the small number of soot particles at these two sites. The parameter n in parentheses represents the total number of soot particles analyzed for each site to calculate D_f and k_g.

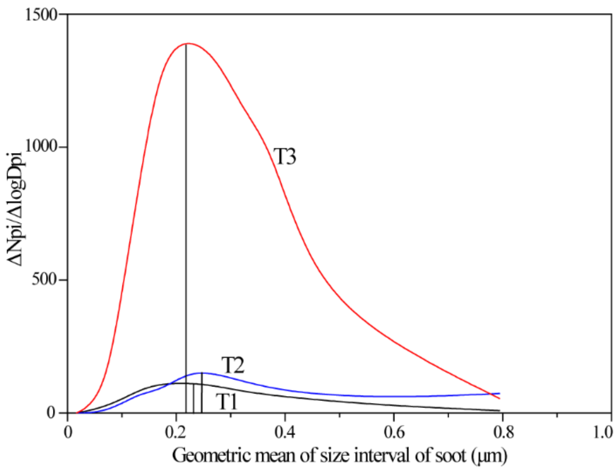

Figure S9. Size distribution of soot core (exclude coating) at T1, T2, and T3.

References

Chi, J. W., Li, W. J., Zhang, D. Z., Zhang, J. C., Lin, Y. T., Shen, X. J., et al. (2015), Sea salt aerosols as a reactive surface for inorganic and organic acidic gases in the Arctic troposphere, *Atmospheric Chemistry and Physics*, *15*(19), 11341-11353.

Rolph, G., Stein, A., and Stunder, B. (2017), Real-time Environmental Applications and Display sYstem: READY, *Environmental Modelling & Software*, *95*, 210-228.